Disturbance and recovery in high speed (110) cleavage in single crystalline silicon

Lv Zhao, Meng Wang, Anne Maynadier, Daniel Nelias

Noname manuscript No.
(will be inserted by the editor)

Disturbance and recovery in high speed (110) cleavage in single crystalline silicon

Lv Zhao · Meng Wang · Anne Maynadier · Daniel Nelias

Received: date / Accepted: date

Abstract Stress perturbations and material defects can significantly affect the fracture initiation and propagation behaviors in brittle materials. In this work, we show that (110) [110] cleavage in silicon deflects onto (111) plane in the presence of contact stresses. The deflection is however not permanent as the crack returns to the (110) plane after a certain length of propagation, even in the case where the crack velocity is up to 78% of the Rayleigh wave speed. The recovery behavior indicates that the (110) [110] cleavage is invariably prevailing when perpendicular to the maximum stress. Following this indication, it can be concluded that the observed (110) [110]–(111) deflection in previous literature is most likely driven by the external disturbance rather than the crack velocity induced toughness evolution. We also highlight that the extra energy for the (110) recovery is minimized at the expense of a large propagation distance upon the plane switch.

Keywords Fracture, silicon single crystal, crack deflection, high speed propagation

1 Introduction

Crystalline silicon occupies a dominant place in the current photovoltaic (PV) applications. However, due to the brittle characteristic, catastrophic failure of the solar cells eventually leads to large power loss and severly impacts reliability and

Lv Zhao
Univ Lyon, INSA-Lyon, CNRS UMR5259, LaMCoS, F-69621, France
E-mail: lv.zhao08@gmail.com

Meng Wang
Univ Lyon, INSA-Lyon, CNRS UMR5259, LaMCoS, F-69621, France

Anne Maynadier
Univ Bourgogne Franche Comté, FEMTO-ST Institute, Departement of Applied Mechanics, CNRS/UFC/ENSMM/UTBM, F-25000, France

Daniel Nelias
Univ Lyon, INSA-Lyon, CNRS UMR5259, LaMCoS, F-69621, France
E-mail: daniel.nelias@insa-lyon.fr

durability of the Si-based PV technology [1,2]. A full understanding on the fracture mechanism in silicon is necessary for the design and the use of PV devices. Albeit continuous investigations have been performed, the fracture behaviors, particularly those manifest during the dynamic propagation, still involve an open discussion [3, 4].

The fracture in silicon mainly takes place along the low energy planes of (110) and (111) [5–8]. The crack velocity in silicon is generally high because of the low fracture toughness and the absence of plastic dissipation under the brittle-ductile transition temperature [9–11]. Among the velocity related fracture phenomena, velocity gap recieved a significant attention. Experiments showed that low (<<2000 m/s) steady state crack velocity was somehow forbidden [6, 12], conversely to the theoretical one that can vary from zero to the Rayleigh wave speed (C_R) according to the linear fracture mechanics. Molecular dynamics simulations explained this threshold as a consequence of a localized phase transformation in the vicinity of the crack tip [13] that delays the fracture initiation. However, a recent work suggested that the velocity gap should not be considered as an universal indication, since an extremely low speed (in 100 m/s speed range) cleavage along (110) can stably take place via kink formation and advance under a suitable temperature and some specific loading conditions [14]. This new finding reveals that the external conditions need to be carefully considered when investigating the fracture in silicon.

As one of the main crack paths in single crystalline silicon, (110) cleavage has been substantially investigated in the previous literature [12,15,16]. Pioneer works highlighted that (110) cleavage involved a directional anisotropy [8,15]. The crack propagation in [001] direction on the (110) plane (denoted as (110) [001]) could not be achieved and the crack systematically switched to (111) plane [7]. This deflection mechanism was elucidated by molecular dynamics simulations [8, 15], which showed that the atom debonding suffered from prounced lattice trapping when heading (110) [001].

Conversely to the (110) [001] cleavage that would yield a global plane deflection, (110) [110] crack manifests with a much higher stability [12]. Mirror-like morphology was observed in the middle of the (110) fracture surface during a high speed propagation (3000 m/s) under tension, accompanied by tiny (111) facets near the specimen surface [12]. This stability was also evidenced in 4-line bending tests (with the crack propagates in the middle of the contact span), in which the (110) plane was dominant up to the propagation velocity of 3700 m/s [16]. However, 3-line bending conditions (with the crack propagates underneath the punch roller) led to disparate fracture scenarios [17, 18]. In these experiments, large (110)–(111) plane deflection was encountered when the crack velocity exceeded 2000 m/s. Regarding the explanation for the deflection phenomenon, the authors conjectured that the (110) dynamic toughness would increase faster than that of the (111) plane when the crack speeds up, so that till a certain velocity (for instance 2900 m/s in the [110] direction) the (110) plane becomes no longer the prevailing crack path in a high speed case [17, 19]. After that, a thermal phonon emission machanism was postulated, which permitted to rationalize the aforementioned conjecture [20]. However, the plane switch theory derived from these 3-line bending tests might not be generalized, since i) the presence of the external perturbations, *i.e.* the contact stresses was not taken into account, and ii) (110) [110] cleavage was revealed stable regardless of the crack velocity (1200 m/s–3700 m/s)

when subjected to pure bending load [16]. From these two attributes, it brings the need for a revision of (110) [110] cleavage, and the fracture stability should be assessed with the careful measures of external perturbations during high speed crack propagations.

Therefore, in the present work, we investigate the (110) [110] initiation and propagation behaviors in the presence of the contact conditions and also with various micro-crack geometries. 4-line bending tests are performed using single crystalline silicon wafer without pre-existing cracks. The absence of pre-cracks not only favors the initiation under the punch roller, but also promotes large crack velocity. High speed camera is used to monitor the first crack, then fractographic anaysis is carried out to identify the cleavage plane and to determine the crack velocity during the propagation. It is observed that the crack tends to switch to the (111) plane at the early propagation stage. However, the disturbance is not permanent as the crack systematically recovers on the (110) plane after a certain length of propagation. Moreover, the recovery occurs over an extremely high velocity (3500 m/s *i.e.* $0.78C_R$). This indicates that the (110) [110] crack path is more energetically favorable than the (111) [1] one in both slow and rapid propagations, which is contradictory to the aforementioned evolution mechanism of the fracture toughness.

2 Experiments

2.1 Single crystalline silicon plate

Solar grade single crystalline silicon was used. The specimens were cut from as-sawn silicon wafers. The dimension of the specimens is 50×50×0.2 mm. The crystal is oriented such that two [110] directions are parallel with the specimen edges and one [100] direction perpendicular to the specimen surface.

As shown in Fig. 1, the specimen surface involves periodic cutting traces and also some hollows (see Fig. 1(a)). The hollows can be more clearly evidenced in Fig. 1(b). This surface morphology is attributed to the diamond wire sawing process where the hard diamond particles indent the new created silicon surface and lead to lateral cracks (manifesting as hollows in Fig. 1(b)). The interaction is shown in the schematic Fig. 1(c). Along with the lateral cracks, sharp median cracks likely nucleate and extend into the material. This kind of cracks, which are barely visible under microscope, have been monitored by X-ray image and shown to have a depth of 10 μm range [21]. These micro-cracks are randomly distributed on the specimen surface.

2.2 4-line bending tests

A 4-line bending set up was used to load the samples til fracture. The silicon plate was placed such that the (110) [110] was right aligned with the punch roller, see Fig. 2. In this configuration, the (110) plane would be the most solicitated as it is perpendicular to the maximum stress. The inner and outer contact spans

[1] In a loading configuration where the maximum stress is perpendicular to the (110) plane.

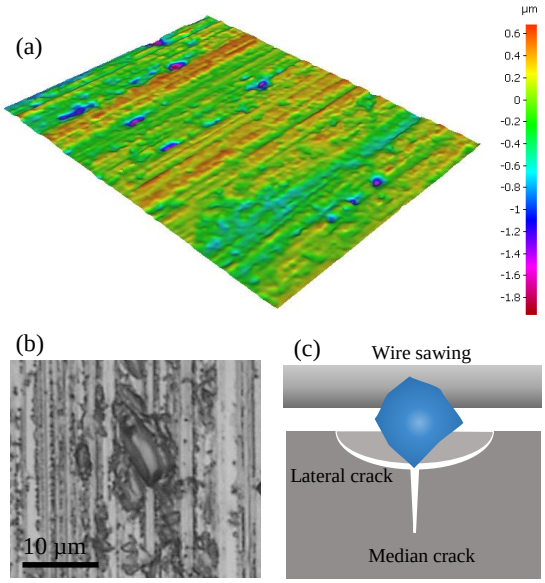

Fig. 1: Morphology of the specimen surface. Distribution of cutting traces and hollows (a), zoom on one hollow (b), schematic drawing of lateral and median cracks induced by diamond particle-material interaction (c).

are 21 mm and 40 mm, respectively. Quasi-static loading conditions with a strain rate in the order of 10^{-6}/s were ensured by a LLOYD-Ametek LFPLUS electro-mechanical machine.

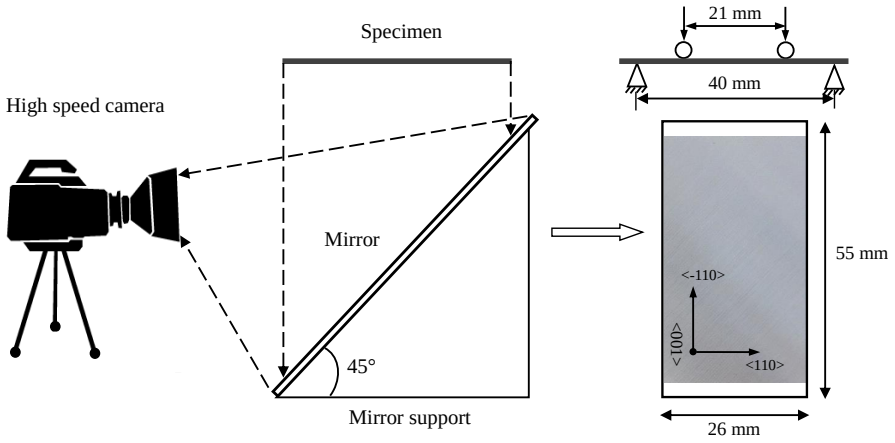

Fig. 2: 4-line bending instrumented with a high speed camera.

2.3 Fracture monitoring

A high speed camera (Photom V710) was set up in order to capture the fracture initiation and propagation. Given that the initiation would most likely occur under the punch roller, the camera was set as it could cover the whole inner contact region, see Fig. 2. As a compromise, the frequency for image acquisition was set to 49000 Hz at the expense of the image resolution (512×256 pixels).

Fractographic analysis was carried out after each test to evaluate in a post-mortem way the cleavage plane as well as the crack velocity. The crack velocity estimation was based on our former work [16], in which a correlation between the crack surface morphology and the propagation velocity was established. In this way, the resolution for velocity measurement was down to micro-scale along the propagation path and the steady state of the crack propagation could be easily identified.

3 Results

The results will be presented in two parts, in each a representative case is addressed. The first one shows the contact perturbations, the second one exhibits the effect induced by the orientation of the fracture origin. For each part, the fracture initiation is highlighted with the high speed imaging technique and the local crack propagation is disclosed with the fractographic analysis. A general discussion on the fracture behavior will finally be carried out in the next section.

3.1 Contact perturbations

The fracture process of the first case is presented in Fig. 3a. The image #0 represents the last photo before cracking. The image #1 monitors the first crack, it involves a subtraction beteween the first photo after cracking and #0. The image #2, which is the second photo after cracking, shows multiple cracks right after the fracture initiation. From #1, it can be noticed that the first crack nucleates and propagates straightly right underneath the punch roller. The image #2 reveals that secondary cracks are curved and involve some branching instabilities. This multiple cracking feature is attributed to a burst of flexural waves that are generated upon the sudden release of the curvature of the bent specimen [22]. The flexural waves then lead to local overstresses and initiate secondary cracks.

According to the obervations on the first crack, the fracture initiation spot and the cleavage planes during the propagation are reconstructed and presented in Fig. 3b. One can notice that the crack initiates from a sub-surface micro-crack which should be induced by the wire sawing. The fracture origin is located near the half length of the specimen, so the crack propagates in two opponent directions. The fracture history for this case is outlined below:

- The fracture initiation takes place on the (110) plane. Very smooth fracture surface can be noticed close to the initiation spot, as shown in the schematic drawing in Fig. 3b. This indicates that the micro-crack is oriented nearly parallel to the (110) plane, which ensures a small mismatch between the fracture origin and the very beginning cleavage path.

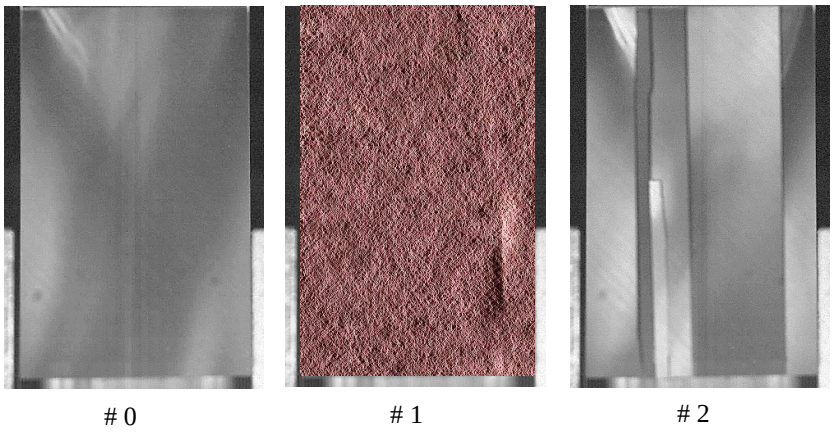

(a)

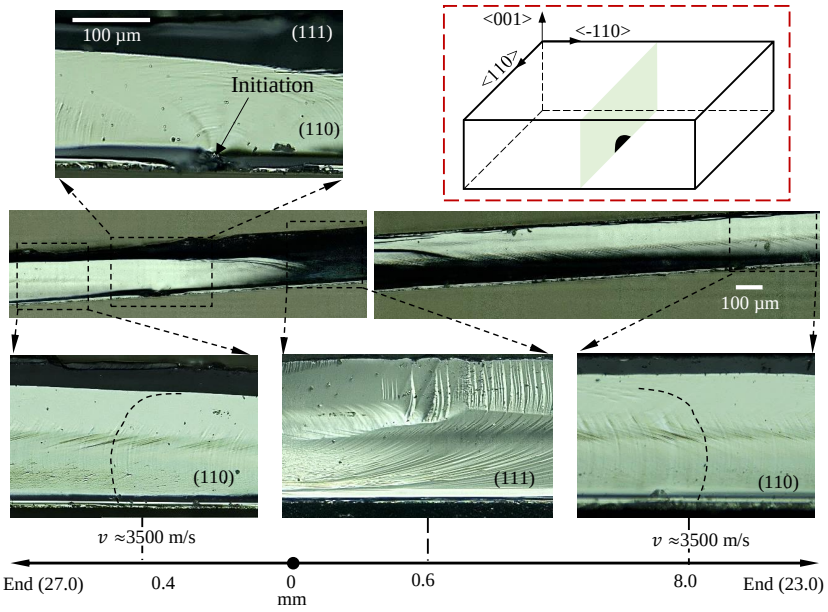

(b)

Fig. 3: Crack deflection and recovery under contact perturbations. First crack monitoring (a), and fractographic reconstruction of the crack initiation and propagation (b). The dotted curved lines in (b) represent the Wallner lines.

– The crack switches to a (111) plane after a very short propagation to the right side, while it remains on the (110) plane during the subsequent propagation. The deflection part manifests as a black zone on the fractography, as can be noticed in the long fractographic images in Fig. 3b.

- After a propagation of about 8 mm to the right side on the (111) plane, the crack returns to the initial (110) plane and then propagates in a steady state. The steady state is clearly indicated by the constant shape of the Wallner lines [16], see Fig. 3b.
- From the morphology of the fracture surface, one can infer that the steady state crack velocties are close for both sides, which are equal to about 3500 m/s. This velocity represents 78% of the Rayleigh wave speed.

The global fracture path for the present case is illustrated in Fig. 4 to show the deflection behaviors. The deflection first nucleates when the crack extends to the compression side of the specimen, this is also where the contact would have strong perturbations in the stress field. This deflection then quickly develops to the tensile side until the (111) plane covers the whole fracture surface. Therefore, it can be concluded that the contact significantly influences the (110) [110] cleavage and utimately leads to a global plane deflection. This conclusion can explain why (111) cleavage was encountered in 3-line bending tests [17].

Fig. 4: Overall fracture path under the contact perturbations.

However, the (110) [110]-(111) deflection is not permanent. According to the observations in the present work, the crack recovers the (110) plane after a certain length of propagation. This recovery was not observed in the previous 3-line bending tests. Interestingly, with other 3 similar tests, it is found that the recovery is repeatable and always takes place at a distance around 8 mm from the initiation point.

3.2 Fracture origin orientation

The present section adresses the second case in which the effect of the fracture origin orientation is involved. The identification of the first crack is presented in Fig. 5a. The numberings #0, #1 and #2 have the same representations as explained in section 3.1. Here, in the image #1, several cracks can be noticed. Among them, the left one, which is right underneath the punch roller, is the longest and therefore considered as the first crack.

Focusing on the first crack, the fracture initiation and propagation are disclosed by fractography, as can be noticed in Fig. 5b. The fracture origin involves also the sub-surface micro-crack, which is located 17 mm away from one of the specimen edges. Following observations are exhibited which allow an overview on the fracture process:

- The crack initiates on the (111) plane. This crack nucleation is due to the fact that the micro-crack orientation is closer to the (111) plane, as indicated in the schematic drawing in Fig. 5b. Yet the contact stresses are not relevant, knowing that the fracture origin is on the tensile side of the specimen and

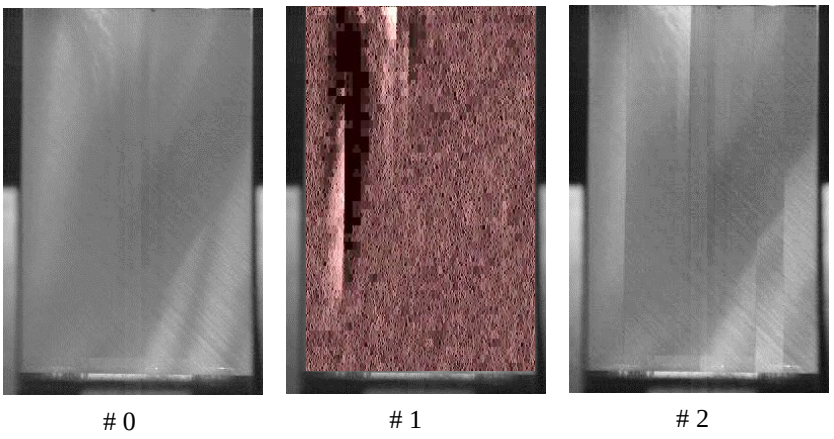

(a)

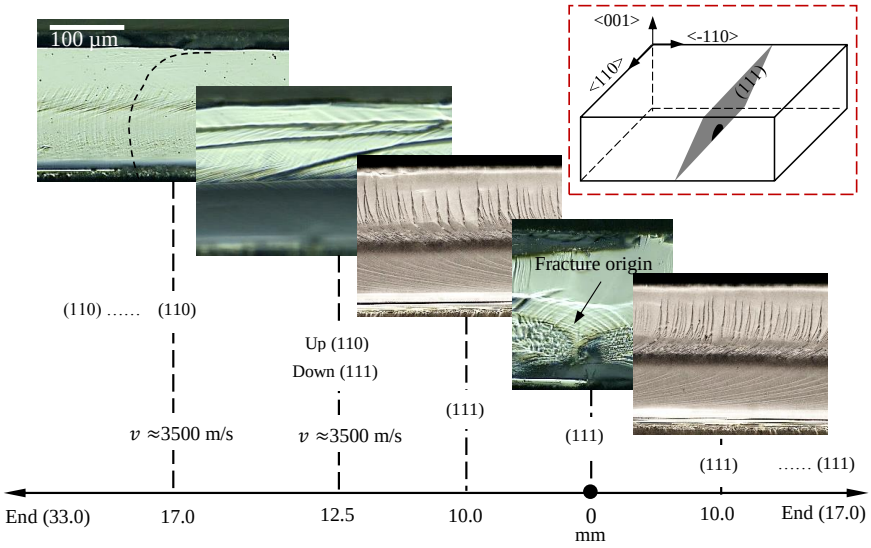

(b)

Fig. 5: Crack deflection and recovery under contact perturbations as well as (111) oriented fracture origin. First crack monitoring (a), and fractographic reconstruction of the crack initiation and propagation (b). The dotted curved lines in (b) represent the Wallner lines.

thus far from the contact perturbations. The crack initiation involves the main difference between the present case and the one presented in section 3.1.

– The crack propagates along the (111) plane to the right side at a quite constant velocity, *i.e.* in its steady state, till reaching one free edge of the specimen. The steady state is revealed by the morphology of the (111) instabilities [23,24], as

shown in the right image in Fig. 5b. The length of the trajectory is about 17 mm.

- To the left side, the crack initially continues with a steady state (111) cleavage. Then, it begins to progressively deflect onto the (110) plane after a propagation length of 12 mm. The deflection is finished at about 17 mm away from the initiation point. The crack then propagates stably on the (110) plane until it reaches the other specimen edge.
- Thanks to the Wallner line shape, the velocity is estimated around 3500 m/s for the (110) part, which reaches nearly 78% of the Rayleigh wave speed. The velocity cannot be inferred on the (111) plane, as the Wallner lines are not noticeable because of the surface instabilities.

The whole crack path for the present case is schematized in Fig. 6. Since both the contact perturbations and the fracture origin-(110) plane mismatch are present in this case, the (111) part is much longer (17 mm) than that in the case where only the contact perturbations are involved (8 mm), see Fig. 3b. It should be noted that the difference is not related to the crack velocity, as the steady state velocities are very close in both cases.

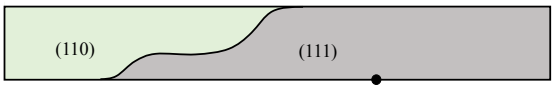

Fig. 6: Overall fracture path under the contact perturbations as well as (111) oriented fracture origin.

Despite of the strong perturbations, the crack jumps to the (110) plane after a long propagation. It should be noted that the deflection process in Fig. 6 is almost the same as that presented in Fig. 4. It begins from the upper portion of the fracture surface and then develops towards the lower portion until the (110) plane covers the whole fracture surface. This deflection behavior will be discussed in the following section.

4 Discussion

Albeit the (111) plane has the smallest fracture toughness ($\Gamma_{(111)}$=2.88 J/m^2), in the present loading configuration (see Fig. 2), the fracture energy dissipation ($\Gamma^*_{(111)}$=3.54 J/m^2) is however larger compared to the (110) plane ($\Gamma^*_{(110)}$=3.46 J/m^2) because of the 35.6° inclination (see Figs. 3b and 5b). Thus, the (110) plane is dominant in low speed fracture (≈1000 m/s), as highlighted in previous works [16–18]. Nonetheless, it still remains unclear on the fracture mechanism in the high speed cases, considering different fracture paths reported when the crack velocity exceeds 2000 m/s [16, 17]. In this work, it has been shown that the crack either stably propagates along the (110) [110] path or switches from the (111) plane to this path at very high velocities (>3000 m/s). It can thus be concluded that the (110) [110] cleavage remains energetically prevailing compared to the (111) one in very high speed cases. In the one hand, this conclusion is coherent with our former

work [16] in which it was found that in the absence of perturbations the crack always chooses the (110) plane for a large range of crack velocites [1200 m/s–3700 m/s]. In the other hand, the dynamic toughness evolution proposed in the previous literature [17, 19] cannot be generalized since it cannot be substantiated by the fracture behavior revealed in our former work [16] as well as the present one.

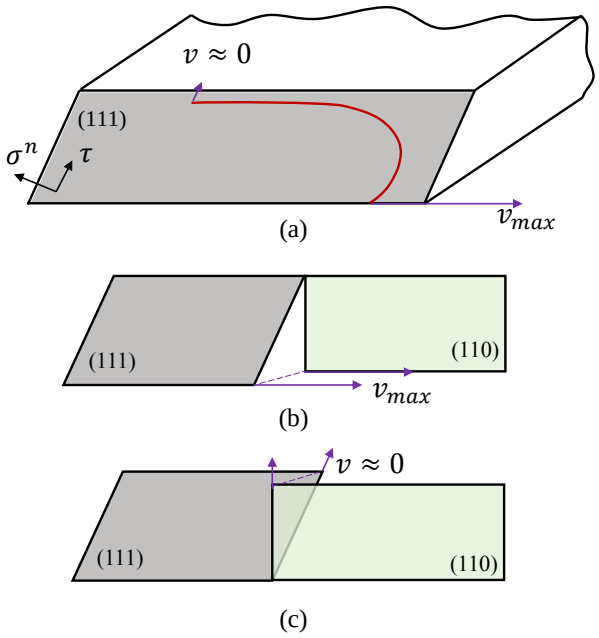

Fig. 7: (111)-(110) deflection. The crack propagates on the (111) plane under bending (a), possibility of deflection from the lower portion (b), and possibility of deflection from the upper portion (c).

As revealed through the experimental results, the contact effect and the (111) oriented defect drive the crack to deflect or initiate on the (111) plane. Then a recovery to the (110) plane takes place as the crack propagates far away from the perturbation origin. However, the (111)–(110) deflection needs extra energy. This can be assimilated to a grain boundary crossing. Previous studies have shown that when a crack switches from one grain to the adjacent one, the misorientation between the two cleavage planes toughens the plane ahead the grain boundary [25]. In this sense, if the deflection is instant or very short, the (110) plane will become no longer favorable since it is toughened due to a rotation of 35.6° ($\Gamma^{**}_{(110)}=\Gamma^{*}_{(110)}/\cos(35.6^\circ)=4.25$ J/m^2 compared to $\Gamma^{*}_{(111)}=3.54$ J/m^2). Therefore, in order to avoid the strong toughening induced by the sudden plane change, the (111)-(110) deflection involves a long process. As indicated in Fig. 4 and Fig. 6, the deflection takes place first in the upper portion of the fracture surface, where the crack velocity is very low, and then extends to the lower portion, where the crack velocity is much higher, until the (110) dominates the whole crack path. The extension covers a propagation length of about 5 mm for both cases presented in

section 3.1 and 3.2. This indicates that the (111)-(110) deflection is likely independent of the previous propagation history.

Why the (111)-(110) deflection initiates from the low speed portion? Indeed, when the crack switches from the (111) plane to the (110) one under bending, there exist two possibilities, as illustrated in Fig. 7. One is that the deflection initiates from the lowest point, where the local velocity coincides with the global velocity and is the largest, see Fig. 7(b), the other is from the highest point, where the local velocity is almost zero, see Fig. 7(c). Assuming that the deflection is instataneous, for the first possibility, the crack needs to rotate twice 90°, while a single rotation of 35.6°is involved for the second one. This clearly shows that the deflection will be much easier to take place from the upper portion in terms of avoding large angle mismatch during the deflection. Moreover, when the deflection begins from the highest point along the crack front, the deflection is naturally progressive as the lower part advances faster and will not be immediately affected by the deflection induced stress rearrangement. The deflection process is shown in the schematic illustration Fig. 8, which permits a full analysis on the local deflection behavior. Taking θ as the angle between the local crack velocity direction and the horizontal direction on the (111) plane, the local velocity direction along the crack front, as indicated by the dotted arrows in Fig.8, can be expressed as:

$$\mathbf{V} = [cos(\theta), sin(\theta), 0] \tag{1}$$

When the deflection towards the (110) plane happens at any point of the crack front, the local velocity direction, as indicated by the solid arrows in Fig.8 becomes:

$$\mathbf{V}' = [cos(\theta), sin(\theta)cos(35.6^\circ), sin(\theta)sin(35.6^\circ)] \tag{2}$$

Therefore, the local deflection angle can be expressed in the function of θ, which is also linked to the position along the crack front, as following:

$$\alpha = acos(cos(\theta)^2 + sin(\theta)^2 cos(35.6^\circ)) \tag{3}$$

As the deflection extends to the lower portion *i.e.* θ varies from 90°to 0°, the deflection angle diminishes until zero at the lowest point, as can be noticed in Fig.9. At the same time, the local velocity v_l increases from zero to the maximum value v_{max} which is also the global crack velocity, as drawn in Fig.9. The local velocity is calculated according to the following approximation:

$$v_l = v_{max} cos(\theta) \tag{4}$$

Thanks to to the Freund condition [26], the energy balance during the crack propagation is well established:

$$G_S = \frac{\Gamma_D C_R}{C_R - v} \tag{5}$$

where G_S denotes the static strain energy release rate, Γ_D represents the dynamic toughness, C_R and v are the Rayleigh speed and the crack velocity, respectively.

It can be noted that higher the crack velocity is, larger the energy dissipation. The relationship can be noticed in Fig. 9. As the deflection angle decreases along with the local velocity increases, the deflection process that described in Fig.8

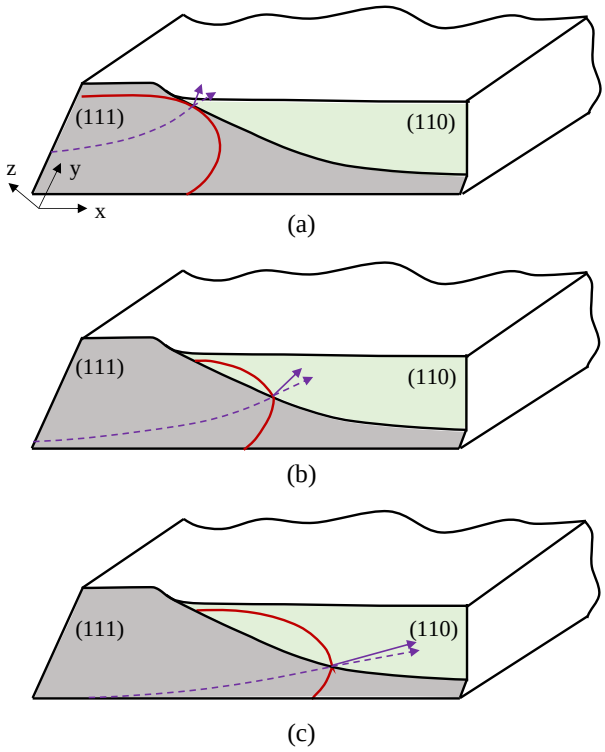

Fig. 8: Schematic process of the (111)-(110) deflection. The crack deflects from the upper portion (a), then it continues to deflect towards the lower portion (b) and (c). The dotted arrows indicate the atom debonding directions upon deflection and the solid arrows stand for the atom debonding directions if the crack remains on the (111) plane.

allows to minimize the extra energy dissipation to jump from the (111) plane to the (110) one. It should be noted that if the deflection starts from the lowest point, the overall dissipated extra energy for plane switch will be much higher, this in turn will strongly decrease the global crack velocity. In other words, the crack deflects from the highest point so that the global crack velocity would not be significantly affected.

To the best of the authors' knowledge, this is the first work showing both the (110)–(111) and the (111)–(110) deflections in the fracture process in silicon. The underlying mechanisms are however different for these two opponent plane switch scenarios. More importantly, the results in the present study raise an open discussion on the previous literature works in which dynamic toughness evolution was assessed [17]. Note also that this study is mainly focused on high speed cracking, which corresponds to large fracture stress and thus large contact force. In the future, the investigation can be completed by other experiments in which controlled fracture orgin size can be ensured to have variant crack propagation velocities.

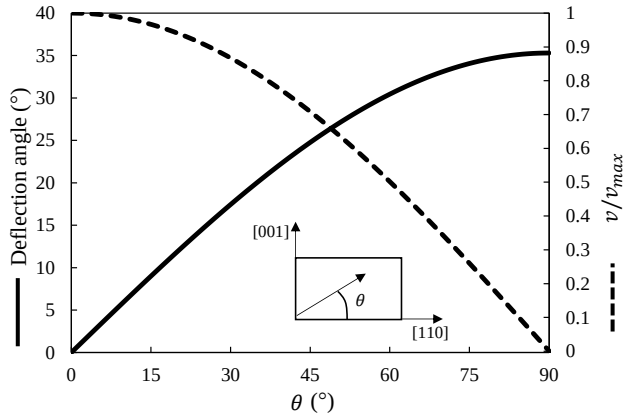

Fig. 9: Deflection angle and local crack velocity evolution along the crack front under bending. The deflection refers to the (111)–(110) cleavage plane switch.

5 Conclusion

In this work, the (110) [110] cleavage in silicon has been investigated in the presence of contact perturbations as well as including various fracture origin geometries. It has been shown that the contact can easily lead to (110)–(111) deflection, which however was previously considered as a consequence of high speed propagation. Albeit the external perturbations deviate the crack from the most favorable path, (111) plane cannot be permanently maintained and the fracture process involves a recovery to (110) [110] scenario during the propagation. This work highligts that the dynamic toughness of the (110) plane should not increase faster than that of the (111) plane until 78% of the Rayleigh wave speed. The (110) plane recovery initiates from the lowest velocity point and progressively extend to the highest velocity point in order to minimize the extra energy dissipation for the deflection.

Acknowledgment

The authors thank the French research agency ANR for partial funding through the DURASOL Equipex project.

References

1. M. Köntges, I. Kunze, S. Kajari-Schröder, X. Breitenmoser, B. Bjørneklett, Sol. Energy Materi. Sol. Cells **95**, 1131 (2011)
2. M. Paggi, I. Berardone, A. Infuso, M. Corrado, Sci. Rep. **4**, 4506 (2014)
3. M. Adda-Bedia, R.E. Arias, E. Bouchbinder, E. Katzav, Phys. Rev. Lett. **110**, 014302 (2013)
4. E. Bitzek, J.R. Kermode, P. Gumbsch, Int. J. Fract. **191**, 13 (2015)
5. A. George, G. Michot, Mater. Sci. Eng. A **164**, 118 (1993)
6. D. Holland, M. Marder, Phys. Rev. Lett. **80**, 746 (1998)
7. F. Ebrahimi, L. Kalwani, Mater. Sci. Eng. A **268**, 116 (1999)
8. R. Pérez, P. Gumbsch, Acta Mater. **48**, 4517 (2000)
9. M. Brede, Acta Metall. Mater. **41**, 211 (1993)
10. J. Samuels, S.G. Roberts, Proc. R. Soc. London, Ser. A, Math. Phys. Sci. **421**, 1 (1989)
11. A. Masolin, P.O. Bouchard, R. Martini, M. Bernacki, J. Mater. Sci. **48**, 979 (2012)

12. T. Cramer, A. Wanner, P. Gumbsch, Phys. Rev. Lett. **85**, 788 (2000)
13. M.J. Buehler, H. Tang, A.C.T. van Duin, W.A. Goddard, Phys. Rev. Lett. **99**, 165502 (2007)
14. J.R. Kermode, A. Gleizer, G. Kovel, L. Pastewka, G. Csanyi, D. Sherman, A.D. Vita, Phys. Rev. Lett. **115**, 135501 (2015)
15. R. Pérez, P. Gumbsch, Phys. Rev. Lett. **84**, 5347 (2000)
16. L. Zhao, D. Bardel, A. Maynadier, D. Nelias, Scr. Mater. **130**, 83 (2017)
17. D. Sherman, I. Be'ery, J. Mech. Phys. Solids **52**, 1743 (2004)
18. D. Sherman, I. Be'ery, Scr. Mater. **49**, 551 (2003)
19. D. Sherman, J. Mech. Phys. Solids **53**, 2742 (2005)
20. F. Atrash, D. Sherman, J. Mech. Phys. Solids **60**, 844 (2012)
21. H.J. Möller, C. Funke, M. Rinio, S. Scholz, Thin Solid Films **487**, 179 (2005)
22. B. Audoly, S. Neukirch, Phys. Rev. Lett. **95**, 095505 (2005)
23. D. Sherman, M. Markovitz, O. Barkai, J. Mech. Phys. Solids **56**, 376 (2008)
24. J. Kermode, L. Ben-Bashat, F. Atrash, J. Cilliers, D. Sherman, A.D. Vita, Nat. Commun. **4**, 2441 (2013)
25. L. Zhao, D. Nelias, D. Bardel, A. Maynadier, P. Chaudet, B. Marie, J. Phys. D. Appl. Phys. **49**(47), 475601 (2016)
26. L.B. Freund, *Dynamic fracture mechanics* (Cambridge University Press, 1990). Cambridge Books Online